Three-dimensional Balance of Cortical Tension and Axial Contractility Enables Fast Amoeboid Migration

Begoña Álvarez-González[1,3], Ruedi Meili[3], Effie Bastounis[1,3], Richard A. Firtel[3,*], Juan C. Lasheras[1,2,4,*], and Juan C. del Álamo[1,4,*,¶]

[1]Department of Mechanical and Aerospace Engineering, University of California, San Diego

[2]Department of Bioengineering, University of California, San Diego

[3]Cell and Developmental Biology, Division of Biological Sciences, University of California, San Diego

[4]Institute for Engineering in Medicine, University of California, San Diego

[*]Co-senior authors
¶To whom correspondence should be addressed: University of California, San Diego, 9500 Gilman Drive, La Jolla, CA 92093-0411, USA, email: Jalamo@ucsd.edu

SUPPORTING MATERIAL

Comparison of the values of the cortical tension that we estimate and the previously measured ones:

The calculated values of the cortical tension for the two wild-type *Dictyostelium* cells shown in Figure 5 are in good agreement with previous measurements obtained from micropipette aspiration experiments that reported an approximate value of 1 mN/m (1-4). In *mhcA*$^-$ cells, we measured a 25% reduction in cortical tension compared to wild-type cells (Figure 5). This reduction is also in agreement with the 20% decrease previously reported for these mutant cells from micropipette aspiration experiments (1), and the 30% reduction estimated by needle poking methods (5). In the *myoA*$^-$*/B*$^-$ cells, we measured a 64% reduction in the cortical tension (Figure 5), also in agreement with previous micropipette aspiration measurements that reported approximately a 60% reduction (2, 6). In the *myoA*$^-$ and *myoB*$^-$ cells, we measured a 12% reduction in the cortical tension (Figure 5), also in agreement with previous micropipette aspiration measurements that reported approximately a 10-15% reduction (2). In filamin null cells, Luo *et al.* found a reduction in cortical tension of approximately 20% using micropipette aspiration (4), whereas in our case, we measure a larger reduction of 46% (Figure 5). Kee *et al.* measured the cortical tension of cortexillin mutant strains using micropipette aspiration. They found that the *cxtB*$^-$ cells had a 16% increase in cortical tension, and that the cortical tension was reduced by 35% and 60% in *cxtA*$^-$ and *cxtA*$^-$*/B*$^-$ respectively (7). In contrast, we found that the *ctxA*$^-$ and *ctxB*$^-$ mutant cells exhibit a decrease of 8% and 5% respectively, and *cxtA*$^-$*/B*$^-$ cells an increase of 10% (Figure 5).

SUPPLEMENTARY FIGURES:

Supplementary figure 1:

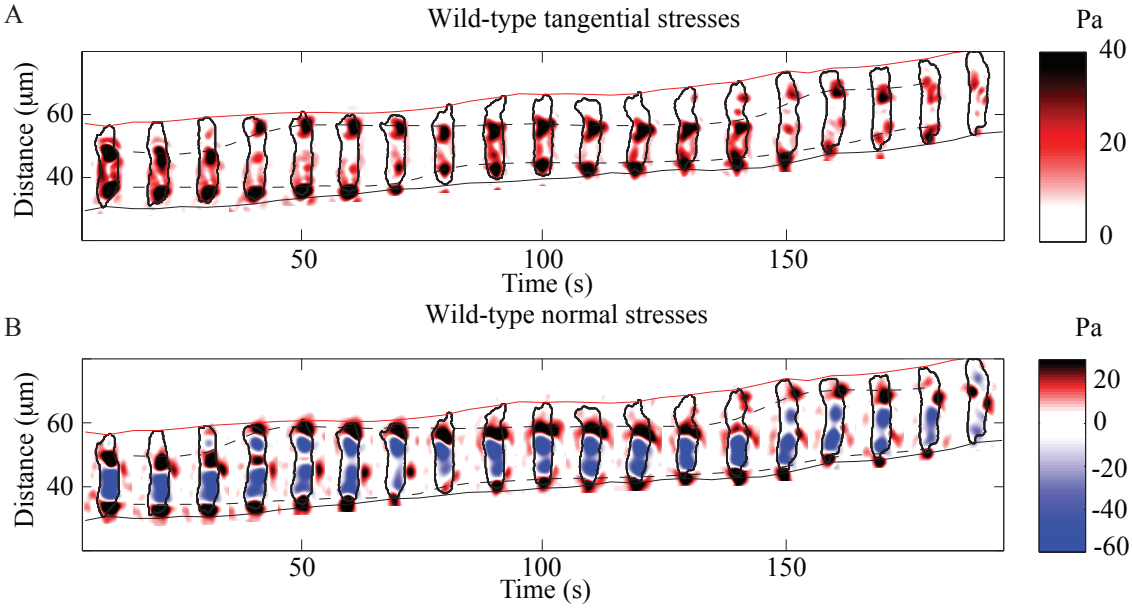

Supplementary figure 1: (A) Spatiotemporal representation of the instantaneous magnitude of the tangential stresses as a function of the position along the cell trajectory and time for a representative wild-type cell. The cell contour is represented in black. The colormap on the right indicates the magnitude of the tangential stresses. The red and black lines indicate the instantaneous front and back edges of the cell respectively. Dotted black lines denote the location of the maximum front and back absolute value of the axial traction tension, $T_x(x, t)$. (B) Same as in panel A for the normal stresses. The colormap on the right indicates the magnitude and direction of the normal stresses. Dotted black lines denote the location of the maximum normal tension $T_z(x, t)$ at the frontal and rear halves of the cell.

Supplementary figure 2:

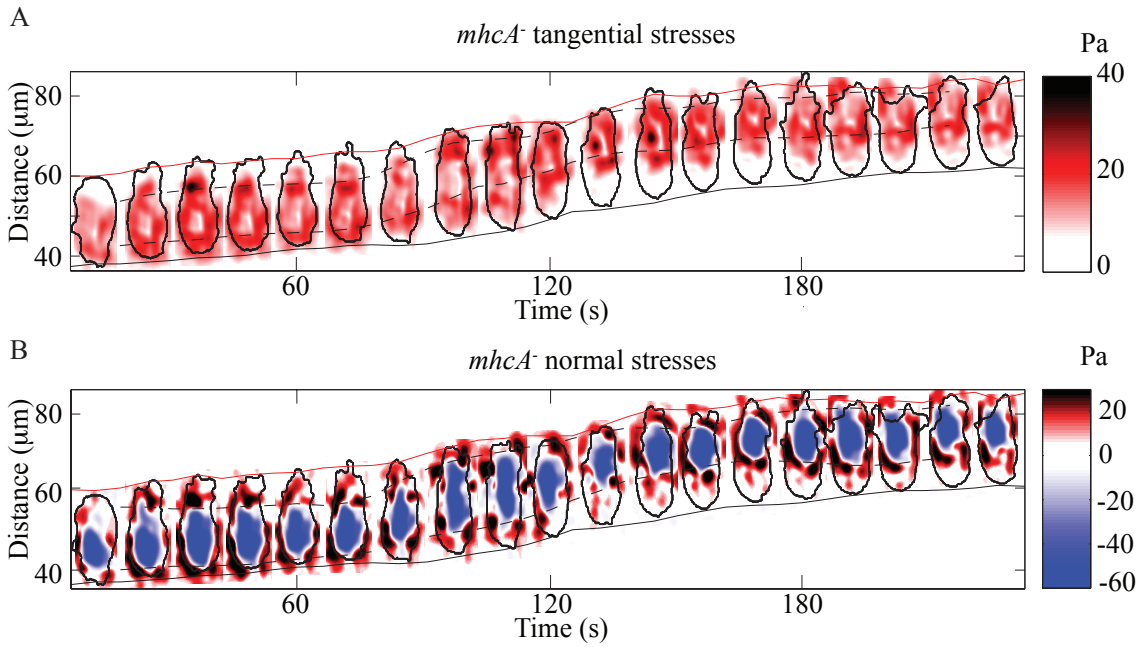

Supplementary figure 2: (A) Spatiotemporal representation of the instantaneous magnitude of the tangential stresses as a function of the position along the cell trajectory and time for a representative *mhcA*$^-$ cell. The cell contour is represented in black. The colormap on the right indicates the magnitude of the tangential stresses. The red and black lines indicate the instantaneous front and back edges of the cell respectively. Dotted black lines denote the location of the maximum front and back absolute value of the axial traction tension, $T_x(x, t)$. (B) Same as in panel A for the normal stresses. The colormap on the right indicates the magnitude and direction of the normal stresses. Dotted black lines denote the location of the maximum normal tension $T_z(x, t)$ at the frontal and rear halves of the cell.

Supplementary figure3:

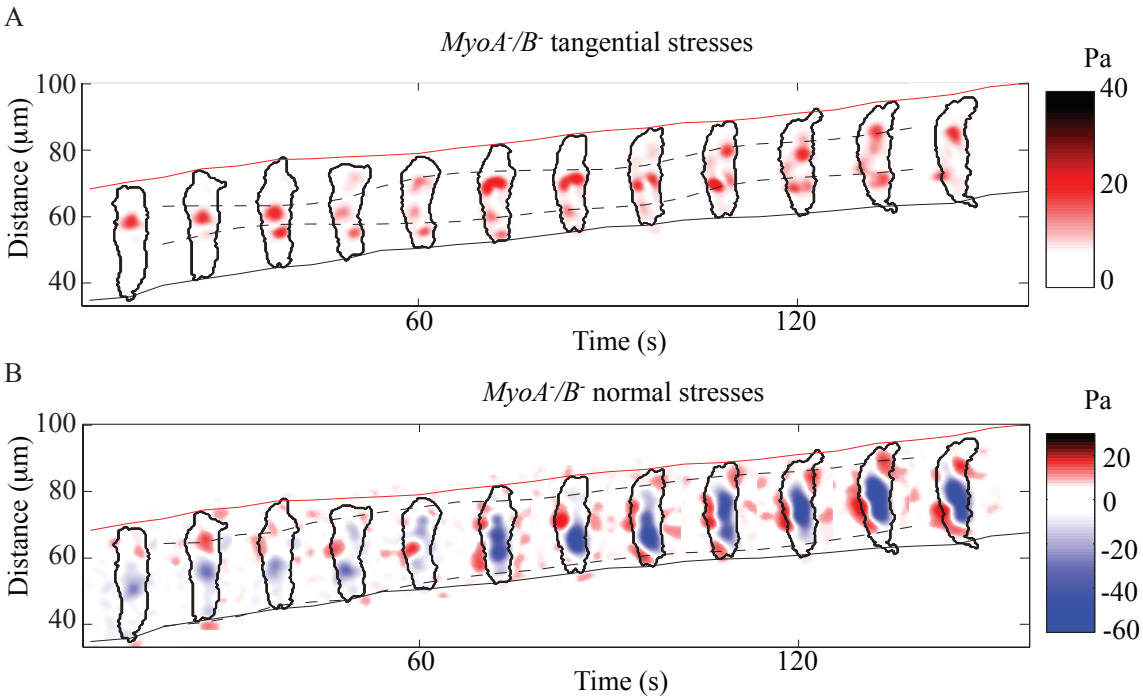

Supplementary figure 3: (A) Spatiotemporal representation of the instantaneous magnitude of the tangential stresses as a function of the position along the cell trajectory and time for a representative *myoA⁻/B⁻* cell. The cell contour is represented in black. The colormap on the right indicates the magnitude of the tangential stresses. The red and black lines indicate the instantaneous front and back edges of the cell respectively. Dotted black lines denote the location of the maximum front and back absolute value of the axial traction tension, $T_x(x, t)$. (B) Same as in panel A for the normal stresses. The colormap on the right indicates the magnitude and direction of the normal stresses. Dotted black lines denote the location of the maximum normal tension $T_z(x, t)$ at the frontal and rear halves of the cell.

Supplementary figure 4:

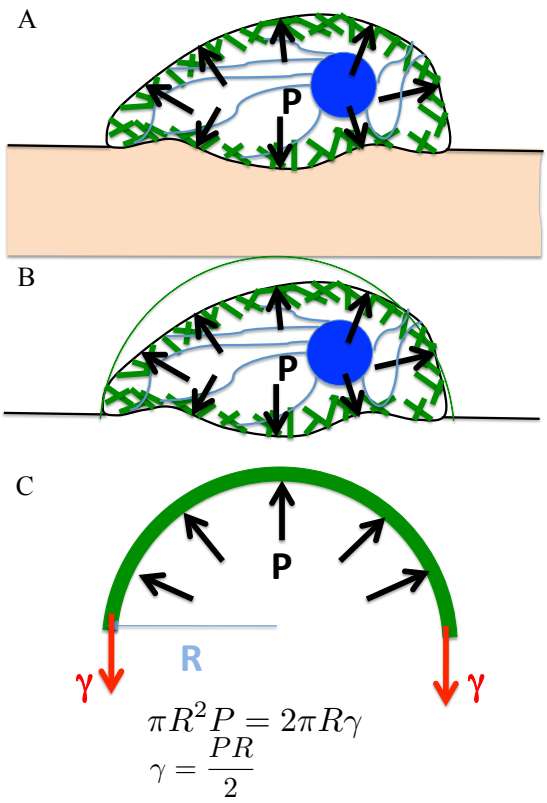

$$\pi R^2 P = 2\pi R\gamma$$
$$\gamma = \frac{PR}{2}$$

Supplementary figure 4: (A) Sketch of a cell that undergoes an internal pressure and exerts a deformation on the substrate while moving. (B) Approximation of the cell shape by a sphere of radius equal to the cell's length. (C) Cortical tension estimation by balancing the force generated by the cortical tension and the internal pressure of the cell.

Supplementary figure 5:

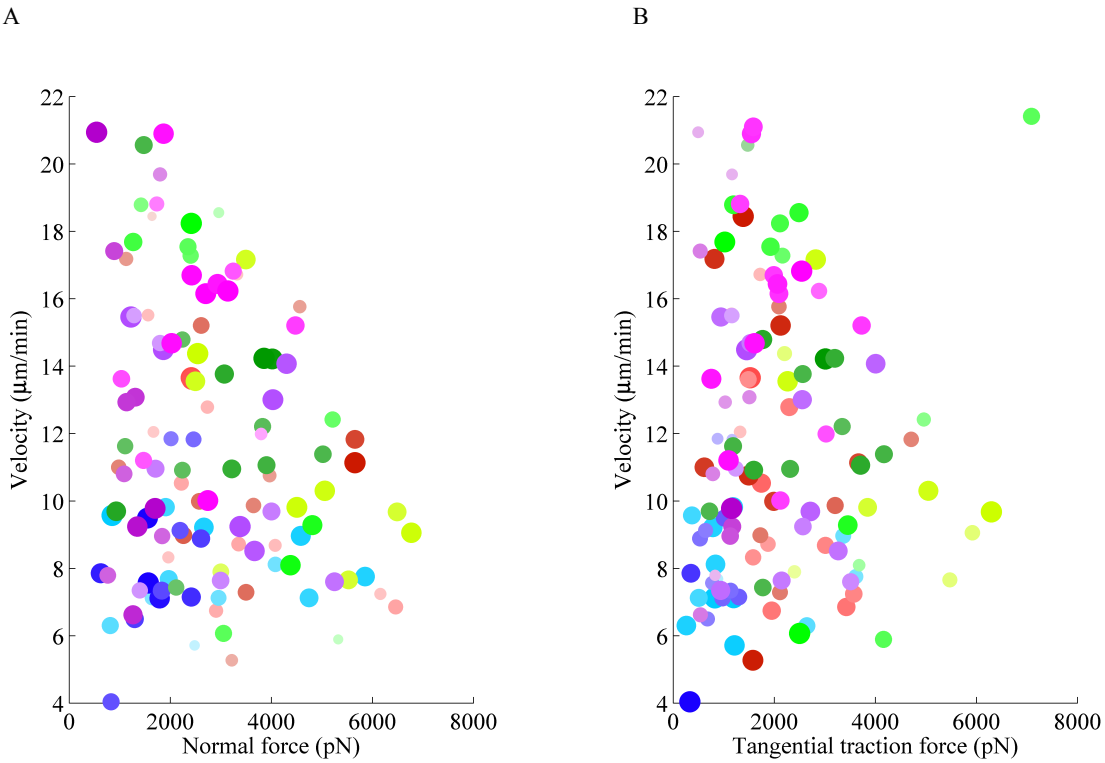

Supplementary figure 5: (A) Scatter plot of the cells' mean velocity versus the average magnitude of the tangential traction forces. (B) Scatter plot of the cells' mean velocity versus the average magnitude of the normal forces. The colors of the circles in the scatter plots for each cell line correspond to the colors used in figure 3. The number of cells for each cell line is the same as in figure 3. To better visualize the correlation, the plane was divided into rectangular tiles of equal area, and size and color of each data point were scaled according to the total number of data points that fall on each specific tile (i.e., its rate of occurrence). As a result, darker, larger circles represent those data points that were observed more often in our experiments, and vice versa.

Supplementary figure 6:

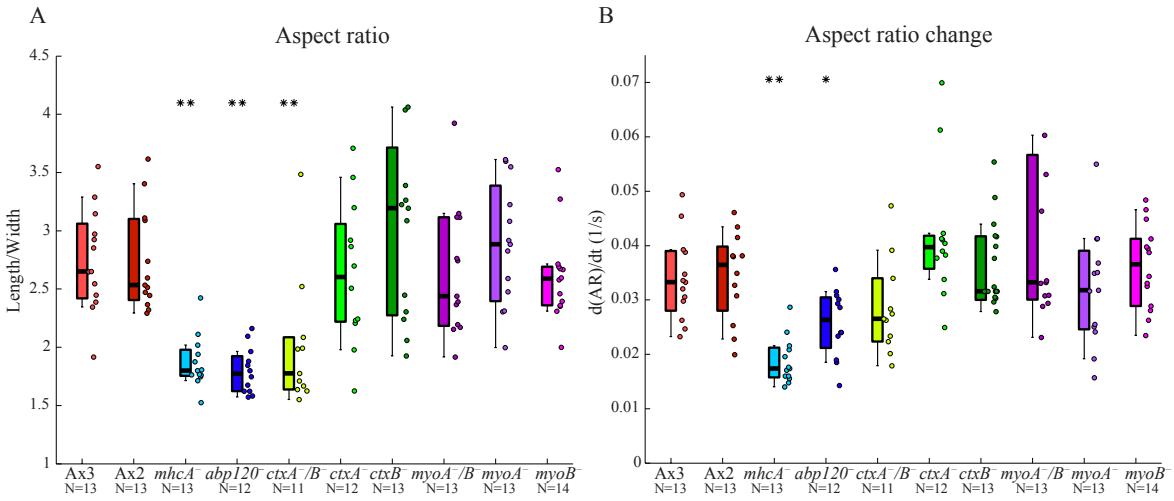

Supplementary figure 6: (A) Cell shape aspect ratio (ratio between the cell length and width) for the cell lines and number of cells (N) indicated. (B) Aspect ratio change with time (derivative of the aspect ratio with respect to the time) for the cell lines and number of cells (N) indicated.

SUPPLEMENTARY MOVIES:

Supplementary movie 1: 3D reconstruction of the actin distribution in a representative chemotaxing wild-type cell expressing *lifeact*-GFP. Z-stacks of fluorescent images were acquired every 6 seconds. The 3D rendering of the actin and the video were generated by using IMARIS software (Bitplane). The movie is accelerated 30x real time.

Supplementary movie 2: 2D projection of the actin distribution for the same cell as in Supplementary movie 1. The 2D projection of the actin and the video were generated by using IMARIS software (Bitplane). The movie is accelerated 30x real time.

Supplementary movie 3: 3D reconstruction of the actin distribution in a representative chemotaxing *ctxA*$^{-}$*/B*$^{-}$ cell expressing *lifeact*-GFP. Z-stacks of fluorescent images were acquired every 6 seconds. The 3D rendering of the actin and the video were generated by using IMARIS software (Bitplane). The movie is accelerated 30x real time.

Supplementary movie 4: 2D projection of the actin distribution for the same cell as in Supplementary movie 3. The 2D projection of the actin and the video were generated by using IMARIS software (Bitplane). The movie is accelerated 30x real time.

Supporting References:

1. Reichl, E. M., Y. Ren, M. K. Morphew, M. Delannoy, J. C. Effler, K. D. Girard, S. Divi, P. A. Iglesias, S. C. Kuo, and D. N. Robinson. 2008. Interactions between myosin and actin crosslinkers control cytokinesis contractility dynamics and mechanics. Curr Biol 18:471-480.
2. Dai, J., H. P. Ting-Beall, R. M. Hochmuth, M. P. Sheetz, and M. A. Titus. 1999. Myosin I contributes to the generation of resting cortical tension. Biophys J 77:1168-1176.
3. Gerald, N., J. Dai, H. P. Ting-Beall, and A. De Lozanne. 1998. A role for Dictyostelium racE in cortical tension and cleavage furrow progression. J Cell Biol 141:483-492.
4. Luo, T., K. Mohan, and P. A. Iglesias. 2013. Molecular mechanisms of cellular mechanosensing. 12:1064-1071.
5. Pasternak, C., J. A. Spudich, and E. L. Elson. 1989. Capping of surface receptors and concomitant cortical tension are generated by conventional myosin. Nature 341:549-551.
6. Titus, M. A. 2000. The role of unconventional myosins in Dictyostelium endocytosis. The Journal of eukaryotic microbiology 47:191-196.
7. Kee, Y. S., Y. Ren, D. Dorfman, M. Iijima, R. Firtel, P. A. Iglesias, and D. N. Robinson. 2012. A mechanosensory system governs myosin II accumulation in dividing cells. Mol Biol Cell 23:1510-1523.